Order-Disorder Transition of Aragonite Nanoparticles in Nacre

Zaiwang Huang and Xiaodong Li*

Department of Mechanical Engineering, University of South Carolina, 300 Main Street, Columbia, South Carolina 29208, USA

(Received 7 November 2011; revised manuscript received 29 February 2012; published 9 July 2012)

Understanding nacre's bottom-up biomineralization mechanism, particularly, how individual aragonite platelets are formed, has long remained elusive due to its crystallographic peculiarity and structural complexity. Here we report that crystallographic order-disorder transition can be triggered within individual aragonite platelets in pristine nacre by means of heat treatment and/or inelastic deformation, offering a unique opportunity to discriminate mysterious aragonite nanoparticles in transmission electron microscopy. Our findings unambiguously uncover why aragonite nanoparticles in pristine nacre have long been inaccessible under TEM observation, which is attributed to the monocrystal-polycrystal duality of the aragonite platelet. The underlying physical mechanism for why an individual aragonite platelet adopts a highly oriented attachment of aragonite nanoparticles as its crystallization pathway is, for the first time, explained in terms of the thermodynamics. The finding of an order-disorder transition in nacre provides a new perspective for understanding the formation for other biominerals.

DOI: 10.1103/PhysRevLett.109.025501 PACS numbers: 61.46.Df, 64.60.Cn, 64.70.qd

Nacre has attracted widespread interest, because its unique hierarchical structure assembled with brittle aragonite (a polymorph of $CaCO_3$) and organic biopolymer leads to several orders of improvement in fracture toughness (in energy terms) compared with its primary counterparts [1–16]. Extensive work has hitherto revealed that nacre is a self-assembled nanocomposite, consisting primarily of highly organized polygonal aragonite platelets with a thickness ranging from 200 to 500 nm and an edge length of about 5 μm sandwiched with 5–20 nm thick organic biopolymer interlayers. A hot debate has been triggered on the structural complexity and crystallographic peculiarity of individual aragonite platelets in nacre. For instance, is an individual platelet made of a single crystal or assembled with nanoparticles? Previous work showed that individual platelets are single crystals and form via epitaxial nucleation [3,4], resulting in a highly stacking sequence layer by layer. Selected area diffraction pattern from TEM further confirmed single-crystal appearance from the crystallographic relationship within single and/or multiple layers [4]. These results, however, sharply conflict with the recent observation that millions of nanoparticles were detected inside one single aragonite platelet by atomic force microscopy [10,17]. Based on two seemingly contradictive observations, the formation mechanism for individual platelets can be ascribed to the screw dislocation-driven growth model [18]. However, how to discriminate the isolated aragonite nanoparticle within platelets under TEM still remains elusive. Here several critical scientific questions are raised: Does nacre cast a ''perfect'' single-crystal platelet using millions of nanoparticles? If yes, why can we not readily detect the ''fused'' boundary or interface between neighboring nanoparticles in TEM? To elucidate these questions is of critical significance to the understanding of nacre's bottom-up self-assembly mechanism and its mechanical strengthening and toughening secrets. Here we design two groups of experiments by heat treatment and inelastic deformation with a purpose to trigger the previously interparallel crystallographic orientation of nanoparticles in pristine nacre. As a result, the emerging disordered nanodomains offer a unique opportunity to discriminate aragonite nanoparticles with an average particle size of a few nanometers. To shed more light on our TEM observation, corresponding *in situ* heat treatment and bending coupled with atomic force microscopy (AFM) were employed to demonstrate the transition of nanoparticle architecture from pristine to heat treated or deformed nacre. Our results clearly unravel that an individual aragonite platelet of nacre is a highly optimized biomineral via highly oriented attachment of aragonite nanoparticles. The ordering process can be rationalized by thermodynamics, rendering a new perspective to understand the formation of highly ordered structure in other biominerals.

In this Letter, natural nacre materials from California red abalone (*Haliotis rufescens*) that belong to the class of gastropoda were chosen for the investigation. The shells were collected alive in Santa Barbara, CA. To minimize the detrimental effect of drying on the structure and mechanical behavior of the shells, they were cleaned and then air delivered in ice to the laboratory where the experiments were conducted. The nacre samples were cut from the nacreous layer of the shells with a water-cooled, low-speed diamond saw. Then the nacre samples were rinsed thoroughly with distilled water. The room temperature TEM samples were prepared by sectioning the nacre using the microtome techniques (Microm HM 325 Rotary Paraffin Microtome). The heat treated and inelastically deformed postmortem powders were immediately collected and dispersed in distilled water with an ultrasonic wave for 2 h.

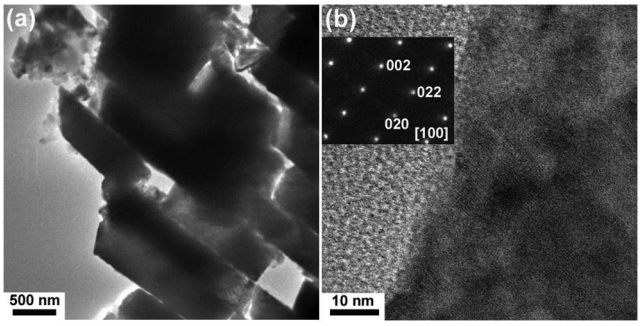

FIG. 1. Ordered microstructure of an aragonite platelet in pristine nacre. (a) Bright-field TEM image showing the brick-mortar microarchitecture. (b) High-resolution TEM lattice fringe image of individual aragonite platelets from (a) exhibiting a single-crystal diffraction pattern (inset).

Both sectioning slice and powder samples were then transferred onto the holey carbon-coated copper film for observation with a JEOL JEM 2100F high resolution TEM at an accelerating voltage of 200 KV. An *in situ* bending test was carried out in a home-built three-point facility, combined with a Veeco Dimension 3100 AFM system (Veeco Metrology Group) for microstructure observation.

Figure 1(a) shows a TEM bright-field image of nacre's brick-mortar microarchitecture from a cross section. The lattice fringe details [Fig. 1(b)] reveal a dense and continuous atomic sequence. Through applying electron diffraction, a single-crystal pattern (inset) is presented, indicating that nacre's growth direction is toward [002] by crystallographic measurement. No additional crystallographic impurity is detected, implying nacre's precise lattice stacking sequence. Meanwhile, the spot diffraction array also means that the crystallographic orientation along the *ab* plane direction, not only for the *c* axis, of the platelet is also highly aligned (the zone axis is [100]). This crystallographic feature is further confirmed by the similar observation from a different zone axis (Supplemental Material [19], Fig. S1). Thus, it seems to be conclusive that we can grant nacre with a single-crystal biomineral.

Based on the above scenario, we designed two pathways to trigger nanoparticle rotation and deformation via routine heat treatment and bending. The previously oriented nanoparticles will give way to a new crystallographic rearrangement. Figure 2(a) reveals a bright-field TEM image of aragonite platelet debris, as scratched from a 350 °C heat treated sample (heat treated in air for 10 min). To rule out the possibility of a phase transformation from aragonite to calcite, the 350 °C heat treated sample was ground into a powder sample for x-ray diffraction (XRD) scanning, where all the peaks can be well indexed as aragonite [Fig. 2(b)]. Our previous results clearly show that metastable aragonite completes the phase transition to calcite until 446 °C [20]. Therefore, it is quite intriguing to see what happens on the microstructure and crystallographic order inside aragonite platelets below this phase transition temperature such as 350 °C. Through examining the electron transparent region, a lattice fringe [Fig. 2(c)] at the edge of the platelet debris is found to be with a hybrid character. Let us select three typical areas [marked by *D*, *E*, and *F* in Fig. 2(c)]; for example, fast Fourier transform (FFT) patterns from corresponding zones *D*, *E*, and *F* are, respectively, presented in Figs. 2(d)–2(f). In Fig. 2(d), the ringlike pattern reveals that the crystallographic arrangement within zone *D* is disordered, and the disordered pattern places a sharp contrast with the results from Fig. 1(b) and Ref. [14]; thus, we suggest that the resulted disordered fringe originates from the imposed heat treatment. As moving to left, i.e., zone *E*, a hybrid crystallographic character [Fig. 2(e)] with both spot and ring marks is presented. Surprisingly, the FFT pattern from zone *F* fully transforms to a spot array without any other crystallographic contamination, indicative of single-crystal-like orientation [Fig. 2(f)]. The gradual order-disorder transition shows that 350 °C heat treatment has

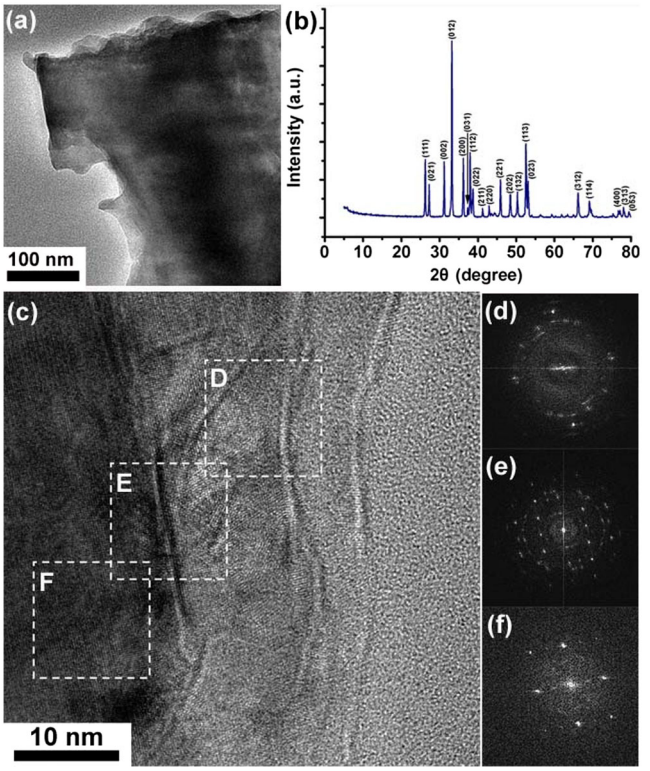

FIG. 2 (color online). XRD spectrum and TEM micrographs of the nacre sample after 350 °C heat treatment. (a) Bright-field TEM image of platelet debris. (b) All XRD peaks can be well indexed as aragonite, showing phase stability of aragonite at 350 °C. (c) Lattice fringe of the platelet exhibiting a hybrid crystallographic feature, through applying the FFT pattern on three typical boxed areas, for example, box areas *D*, *E*, and *F*, the corresponding crystallographic orientation [(d)–(f)] presenting a gradual transition from polycrystalline to monocrystalline appearance.

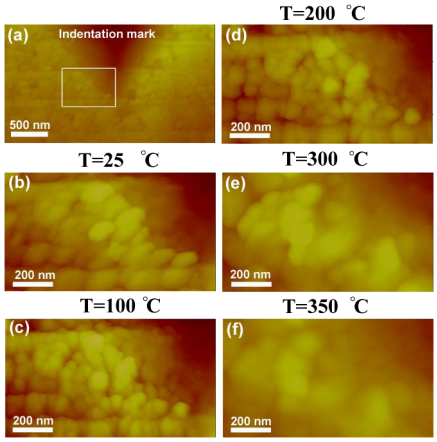

FIG. 3 (color online). AFM evolution observation of aragonite nanoparticles under different temperatures. (a) A reference mark was made by Vickers indentation on the cross section of nacre, where an interesting area enclosed by a white box was selected for AFM observation. (b)–(f) are a series of AFM amplitude images by means of heat treatments at T = 25, 100, 200, 300, and 350 °C; a sharp shift of nanoarchitecture involving nanoparticle coarsening, reorientation can be detected at a relatively high temperature, i.e. 300 and 350 °C, whereas there is no obvious change at 25, 100, and 200 °C.

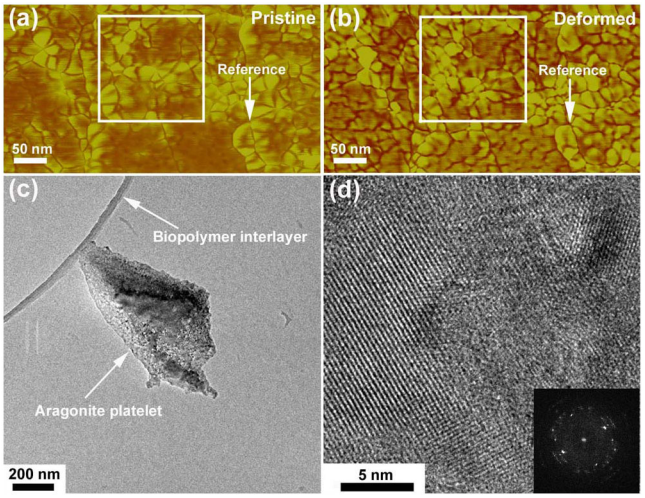

FIG. 4 (color online). Microstructure observation of aragonite nanoparticles. (a),(b) AFM nanoparticle observation within an interesting area (white box enclosed) from pristine and deformed nacre (three-point bending), showing the change in nanoparticle architecture. After that, a TEM sample was prepared from a severely deformed sample (3% flexural strain). (c) Aragonite platelet fragment adhering to a biopolymer interlay (arrowed). (d) Disordered nanoparticle arrangement from inside the platelet scatters a polycrystalline pattern (inset), showing an order-disorder crystallographic transition upon inelastic deformation.

imposed an effect on the edge region of the platelet via triggering the reorientation of aragonite nanoparticles. To obtain a real-time evolution process of nanoparticle architecture, we carried out *in situ* heating experiments at a series of temperatures, i.e., 100, 200, 300, and 350 °C, as shown in Fig. 3. For *in situ* imaging, a Vickers indentation mark was made on the cross section for reference [Fig. 3(a)], where an interesting area (white box enclosed) was selected for AFM imaging. At 100 and 200 °C, no obvious temperature effect is detected on the nanoparticle arrangement [Figs. 3(c) and 3(d)] compared with the pristine status [Fig. 3(b)]. With increasing the temperature to 300 [Fig. 3(e)] and 350 °C [Fig. 3(f)], a sharp shift of nanoparticle architecture is provoked, which might be explained as grain coarsening and/or crystal reorientation. Based on the observation, we thus conclude that the observed nanoparticles [Fig. 2(c)] originate from a pristine aragonite platelet without phase transition occurrence.

Additionally, we also probed the effect of inelastic deformation on the order-disorder transition of aragonite nanoparticles. *In situ* three-point bending [21] in conjunction with AFM are utilized to observe a change of the nanoparticle architecture inside a pristine [Fig. 4(a)] to deformed [Fig. 4(b)] platelet. Clearly, the remarkable change of nanoparticle morphology is in excellent agreement with the order-disorder transition. After bending (3% flexural strain), the deformed sample was used to prepare a TEM powder sample using the scratch method (peeling off along the *ab* plane). The bright-field image [Fig. 4(c)] shows that postmortem debris adheres to the biopolymer chain. Figure 4(d) obviously demonstrates a lattice image where aragonite particles are arranged in a disordered fashion, in sharp contrast with those in Fig. 1(b). The random crystallographic orientation is further confirmed by the ringlike FFT pattern (inset). This result suggests that the previously interparallel aragonite nanoparticles have given way to random orientation.

Figure 5 is a two-dimensional schematic illustration that an order-disorder transition [(a) to (b)] can be initiated through temperature or deformation. The crystallographic evolution can be derived from the well-recognized fact that aragonite nuclei crystallize into several-nanometer-sized particles from molecular attachment [22] and subsequently self-assemble into pseudo single crystal (sharing the same orientation) via reducing the surface energy [23].

Thermodynamically, we consider the aragonite nanoparticle self-assembly as a thermodynamic system with constant pressure and temperature:

$$\Delta G = \Delta V \cdot P - T \cdot \Delta S, \quad (1)$$

where ΔG is the change of Gibbs free energy and P, ΔV, T, and ΔS are the pressure, system free volume change (free volume refers to the available space after nanoparticle packing [24]), absolute temperature, and entropy change, respectively. Apparently, the spontaneous self-assembly process can lead to a decrease of Gibbs free energy ($\Delta G < 0$) [18], accompanied with the high ordering of aragonite nanoparticles, as validated by TEM observation [18,25]. In this regard, it seems to be counterintuitive that

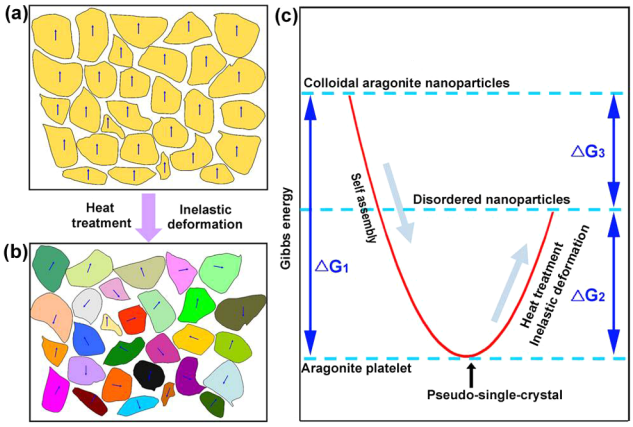

FIG. 5 (color online). Order-disorder transition of the aragonite nanoparticle arrangement. (a) Aragonite nanoparticles are self-assembled into a pseudo-single-crystal platelet (sharing the same orientation). (b) Upon imposing external effects, i.e., heat treatment and/or inelastic deformation, nanoparticles are rearranged in a random manner. (c) The disordered colloidal aragonite nanoparticles self-assembled into an ordered aragonite platelet via decreasing the Gibbs energy ($\Delta G_1 < 0$). Upon imposing an external effect, i.e., heat treatment and/or inelastic deformation, the Gibbs energy will accordingly increase ($\Delta G_2 > 0$) but cannot rebound to the previous state ($|\Delta G_2| < |\Delta G_1|$). The excess energy ($\Delta G_3$) can be derived from the amount of grain boundary bonding energy, relative to the free colloidal aragonite nanoparticles.

spontaneous self-assembly reaction should be towards disordering (entropy increase based on the third law of thermodynamics). How does the system realize the ordering without external work? Pioneering work by Onsager [26] has shown that the compensation entropy due to free volume change ($\Delta V < 0$) from initial disordering to final ordering can be more than the entropy loss associated with the ordering process. That is, the thermodynamically spontaneous process ($\Delta G < 0$) in Eq. (1) can be realized because of the highly oriented attachment ($\Delta V < 0$), although the ordering process induces the decrease of system entropy. Conversely, when a temperature effect (i.e., 350 °C) is imposed upon the ordering system under a constant pressure, the endothermic reaction [20] prior to the occurrence of phase transition to calcite can raise the Gibbs free energy ($\Delta G > 0$):

$$\Delta G = \Delta V \cdot P - T \cdot \Delta S - S \cdot \Delta T, \qquad (2)$$

where S is the system entropy ($S > 0$ above absolute zero temperature) and ΔT is the temperature change ($\Delta T > 0$). The reaction is inherently accompanied by the entropy increase ($\Delta S > 0$) due to the disordering, implying that the free volume expansion of an aragonite platelet has to be compensated ($\Delta V > 0$) despite no experimental evidence on hand, while upon mechanical deformation with invariable temperature and pressure, the increase of Gibbs free energy ($\Delta G > 0$) can be translated by the energy in the form of external work arising from deformation. Similarly, the deformation-induced crystallographic transition due to disordering can increase entropy ($\Delta S > 0$). Therefore, based on Eq. (1), the free volume will accordingly expand ($\Delta V > 0$), as evidenced by the nanoparticle rotation or reorientation from ordering to disordering [21]. Significantly, the increased Gibbs free energy (ΔG_2 in Fig. 5) associated with the heat treatment or mechanical inelastic deformation is smaller than ΔG_1 (ΔG_1 is the energy loss from disordered colloidal aragonite nanoparticles to a highly ordered aragonite platelet). The excess energy (ΔG_3) can be ascribed to the amount of Gibbs energy change from colloidal nuclei to the aragonite platelet with disordered aragonite nanoparticles ($\Delta G_3 = \Delta G_1 - \Delta G_2$), where the disordered aragonite nanoparticles are bonded together by a grain boundary, relative to the free surface at the colloidal state.

Based on the aforementioned results, several aspects should be noted. First, conventional methods for fabricating nanostructured metallic materials need a hypercritical method or condition, i.e., surface mechanical attrition treatment [27], high pressure torsion [28], or severe plastic deformation [29]. Here, our observed nanoparticles remain comparatively easier to be acquired by medium temperature (350 °C) and routine mechanical deformation. Moreover, we notice that particle size is in the regime of a few nanometers, which is sharply different from that achieved in engineered materials through using modern top-down techniques. This can be explained only by the fact that aragonite nanoparticles in biomineral nacre are readily rearranged in a disordered manner owing to a relatively active or weak boundary. Second, to rule out the possibility that an artificial factor in the scratch process may affect the microstructure of fragment in Fig. 4(c), we show another case that a TEM sample from pristine nacre is also prepared by the same method (Supplemental Material [19], Fig. S2). The results demonstrate that the scratch process using a razor blade has no effect on the microstructure, as evidenced by the single-crystal diffraction pattern. Third, we suggest that it is quite difficult to discriminate aragonite nanoparticles in pristine nacre under TEM, because the crystallographic orientation is highly aligned. TEM results with single-crystal appearance have independently been reported by several different methods, i.e., focused–ion-beam fabrication [10], ion milling [11], and microtome sectioning [18]. All previous TEM observations showing single-crystal character are not contradictive with our explanation, as proposed by the monocrystal-polycrystal duality of aragonite platelet. However, our viewpoint, at least, is a coexistence perspective for aragonite platelet formation relative to the epitaxial growth mode [3,4]. Fourth, self-assembly biominerals often show single-crystal-like nanocrystalline aggregation, i.e., brittle star [30,31], which can be regarded as an imperfect single crystal. There exists a

long-range topological ordering, but it may lose short-range ordering owing to grain boundary-interface transition and biopolymer impurity (amorphous aggregation). A similar crystallographic model was recently reported in metallic glasses under high pressure [32].

We thank R. Z. Wang for providing the nacre samples and Dr. Douglas Blom at the University of South Carolina EM Center for TEM technical support. This work was supported by the U.S. Army Research Office under Grant No. W911 NF-07-1-0449 and the University of South Carolina NanoCenter.

*Corresponding author.
lixiao@cec.sc.edu

[1] J. D. Currey, Proc. R. Soc. B **196**, 443 (1977).
[2] A. P. Jackson, J. F. V. Vincent, and R. M. Turner, Proc. R. Soc. B **234**, 415 (1988).
[3] S. W. Wise, Science **167**, 1486 (1970).
[4] Q. L. Feng, F. Z. Cui, G. Pu, R. Z. Wang, and H. D. Li, Mater. Sci. Eng., C **11**, 19 (2000).
[5] R. Menig, M. H. Meyers, M. A. Meyers, and K. S. Vecchio, Acta Mater. **48**, 2383 (2000).
[6] R. Z. Wang, Z. Suo, A. G. Evans, N. Yao, and I. A. Aksay, J. Mater. Res. **16**, 2485 (2001).
[7] H. J. Gao, B. Ji, I. L. Jäger, E. Arzt, and P. Fratzl, Proc. Natl. Acad. Sci. U.S.A. **100**, 5597 (2003).
[8] E. Munch, M. E. Launey, D. H. Alsem, E. Saiz, A. P. Tomsia, and R. O. Ritchie, Science **322**, 1516 (2008).
[9] Z. W. Huang, H. Z. Li, Z. L. Pan, Q. M. Wei, Y. J. Chao, and X. D. Li, Sci. Rep. **1**, 148 (2011).
[10] M. Rousseau, E. Lopez, P. Stempflé, M. Brendlé, L. Franke, A. Guette, R. Naslain, and X. Bourrat, Biomaterials **26**, 6254 (2005).
[11] F. Barthelat, C.-M. Lia, C. Comia, and H. D. Espinosa, J. Mater. Res. **21**, 1977 (2006).
[12] S. K. Katti, B. Mohanty, and D. R. Katti, J. Mater. Res. **21**, 1237 (2006).
[13] C. Ortiz and M. C. Boyce, Science **319**, 1053 (2008).
[14] N. Nassif, N. Pinna, N. Gehrke, M. Antonietti, C. Jäger, and H. Cölfen, Proc. Natl. Acad. Sci. U.S.A. **102**, 12 653 (2005).
[15] J. H. E. Cartwright, A. G. Checa, B. Escribano, and C. I. Sainz-Díaz, Proc. Natl. Acad. Sci. U.S.A. **106**, 10 499 (2009).
[16] A. G. Checa, J. H. E. Cartwright, and M.-G. Willinger, Proc. Natl. Acad. Sci. U.S.A. **106**, 38 (2009).
[17] X. D. Li, W.-C. Chang, Y. J. Chao, R. Wang, and M. Chang, Nano Lett. **4**, 613 (2004).
[18] X. D. Li and Z. W. Huang, Phys. Rev. Lett. **102**, 075502 (2009).
[19] See Supplemental Material at http://link.aps.org/supplemental/10.1103/PhysRevLett.109.025501 for more TEM observations.
[20] Z. W. Huang and X. D. Li, Mater. Sci. Eng., C **29**, 1803 (2009).
[21] X. D. Li, Z. H. Xu, and R. Z. Wang, Nano Lett. **6**, 2301 (2006).
[22] E. M. Pouget, P. H. H. Bomans, J. A. C. M. Goos, P. M. Frederik, G. de With, and N. A. J. M. Sommerdijk, Science **323**, 1455 (2009).
[23] R. L. Penn and J. F. Banfield, Science **281**, 969 (1998).
[24] H. N. W. Lekkerkerker and A. Stroobants, Nature (London) **393**, 305 (1998).
[25] K. Takahashi, H. Yamamoto, A. Onoda, M. Doi, T. Inaba, M. Chiba, A. Kobayashi, T. Taguchi, T. Okamura, and N. Ueyama, Chem. Commun. (Cambridge) **8**, 996 (2004).
[26] L. Onsager, Ann. N.Y. Acad. Sci. **51**, 627 (1949).
[27] K. Y. Zhu, A. Vassel, F. Brisset, K. Lu, and J. Lu, Acta Mater. **52**, 4101 (2004).
[28] Y. Ivanisenko, W. Lojkowski, R. Z. Valiev, and H.-J. Fecht, Acta Mater. **51**, 5555 (2003).
[29] R. Z. Valiev, R. K. Islamgaliev, and I. V. Alexandrov, Prog. Mater. Sci. **45**, 103 (2000).
[30] J. Aizenberg, A. Tkachenko, S. Weiner, L. Addadi, and G. Hendler, Nature (London) **412**, 819 (2001).
[31] J. Aizenberg, D. A. Muller, J. L. Grazul, and D. R. Hamann, Science **299**, 1205 (2003).
[32] Q. S. Zeng, H. Sheng, Y. Ding, L. Wang, W. Yang, J.-Z. Jiang, W. L. Mao, and H.-K. Mao, Science **332**, 1404 (2011).